A microfluidic approach for investigating multicomponent system thermodynamics at high pressures and temperatures

Bruno da Silva Pinho, Stéphane Girardon, Frédéric Bazer-Bachi, Ghislain Bergeot, Samuel Marre, Cyril Aymonier

A microfluidic approach for investigating multicomponent system thermodynamics at high pressures and temperatures

Bruno Pinho,[ab] Stéphane Girardon,[a] Frédéric Bazer-Bachi,[a] Ghislain Bergeot,[a] Samuel Marre[b] and Cyril Aymonier*[b]

DOI: 10.1039/XXXXXX

In this work, we present a novel microfluidic-based approach for investigating the thermodynamics of multicomponent systems at high pressures and temperatures, such as determining miscibility diagrams and critical coordinates of complex mixtures. The developed method is primarily based on (i) bubble and dew point detection through optical characterization and (ii) the use of a so-called dynamic stop-flow measurement mode for fast screening of the diagram parameters, mainly *P*, *T* and composition. Our strategy was validated through the studies of model binary CO_2–alkane mixtures. The obtained results were then compared to PREOS-calculated and literature data. We later applied this strategy for determining ternary and quaternary mixtures critical coordinates. This approach has equal accuracy compared to conventional high-pressure optical cell methods but allows for a much faster phase diagram determination, taking advantage of improved heat and mass transfers on the microscale and of the dynamic stop-flow approach.

1. Introduction

The knowledge associated with phase behavior is of primary interest for various industrial applications. Getting to know whether a complex fluid mixture will be multiphasic or monophasic depending on the operating parameters and the reaction profile is crucial data required by chemical engineers to build up their process, in particular when considering high-pressure/high-temperature systems. In relation to phase behaviors, supercritical fluids[1–4] (pressure and temperature conditions above the critical point – P_c, T_c) have attracted much interest because of their unique properties: liquid-like densities and gas-like viscosities and diffusivities,[5] which can be continuously adjusted by small changes in temperature and pressure to fit the process needs.

Traditionally, phase diagrams and critical coordinates are obtained with chromatography techniques[6] and/or high pressure optical cell (HPOC) measurement methods[7,8] using isochoric or dynamic methods.[9] Although these methods can lead to very precise and reliable thermodynamic data, they are also highly time-consuming. These limitations are mainly due to the macroscale volumes that need to reach equilibria (temperature, composition, *etc.*) before any measurements can be performed. Performing phase behavior analysis in microfluidic devices is emerging and aims at replacing these traditional approaches. Nowadays, phase microscale behavior analyses at high pressures and temperatures are possible because the microfluidic knowledge has evolved towards the microfabrication of devices that can handle such harsh conditions,[10] the development of supercritical microfluidics,[11] the modeling of supercritical microflows[12] and the understanding of pressure drops in microscale networks.[13] All of this knowledge opened space for conducting on-chip phase behavior studies, which require advanced control of the operating parameters (pressure, temperature and composition). Compared to conventional techniques, microfluidic approaches can add huge benefits, providing low reagent consumption, fast screening, low operating times (97% time reduction compared to conventional pressure–volume–temperature (*PVT*) techniques[14]) and the ability to implement *in situ* analysis techniques.[15,16] Furthermore, the ability to work in continuous flow mode allows solving hydro/mass transfer/thermodynamic problems simultaneously through on-chip μPIV,[17] mass transfer analysis[18,19] and *PVT* diagram construction.[14]

The first published approach to study on-chip phase behavior was proposed by Mostowfi *et al.*[14] In their work, the authors successfully developed a microdevice equipped with fluidic restrictions inside the microchannel responsible for droplet nucleation, assuring a fast equilibrium state after fluid restriction. It was used to investigate binary phase *PVT* diagrams using integrated membrane-based optical sensors

[a] *IFPEN, Rond-Point de l'Echangeur de Solaize, 69390 Solaize, France*
[b] *CNRS, Univ. Bordeaux, ICMCB, F-33600, Pessac, France.*
E-mail: aymonier@icmcb-bordeaux.cnrs.fr; Fax: +0033 5 40 00 27 61; Tel: +0033 5 40 00 26 72

for *in situ* pressure measurements. Fluid phase behavior was analyzed at equilibrium using flow visualization to determine gas–liquid volume fractions depending on temperature and pressure. These data provide sufficient information to construct binary phase diagrams. More recently, Fisher *et al.*[19] used the same principle to investigate hydrocarbon equilibrium in oil. Good agreement was obtained when compared to pycnometer flash experiments. In both cases, the microsystem inside pressure was maintained due to high pressure drop channels at the microsystem outlet, meaning the pressure was flow rate dependent. To some extent, this could potentially affect the time to reach phase equilibrium, reducing the contact time between phases at high flow rates, although the authors proposed to use microchannels with a small hydraulic diameter allowing screening an acceptable range of pressure by small changes in flow rates.

In this general context, this paper presents a novel strategy to conduct on-chip multicomponent phase behavior studies at high pressures ($1 < P$ (bar) < 200) and temperatures ($300 < T$ (K) < 500). The developed method is primarily based on (i) bubble and dew point detection through optical characterization and (ii) the use of a so-called dynamic stop-flow measurement mode for fast screening of the operating parameters. The proof of concept is demonstrated through the determination of phase diagrams and critical locus curves for benchmark binary (alkanes + CO_2) and ternary (alkanes + CO_2 + H_2) mixtures. These mixtures were chosen as model mixtures for they are commonly used in industry, relatively stable under high pressure and high temperature conditions (no reactivity between components) and have existing literature data available for comparison.

The first section of the manuscript briefly discusses the microsystem design and set-up and the general strategy employed. We then expose the obtained experimental results, which are later compared with literature and numerical data calculated with the Peng–Robinson equation of state (PREOS).

2. Experimental section

Chemicals

Cyclohexane and pentane (both 99.5% purity) were purchased from Sigma-Aldrich® and used as received. Carbon dioxide, hydrogen and propylene were purchased from Air Liquide®.

Microsystem design

We developed a silicon/Pyrex microsystem fabricated using standard lithography/dry etching techniques.[10] The microsystem exhibits rectangular channels with dimensions of 200 μm and 100 μm for width and depth, respectively (*i.e.* hydraulic diameter of 133 μm). The microchannel has a total length of 1 m with rounded edges. The overall design leads for instance to a pressure drop of 0.8 bar when considering pure cyclohexane flowing at 50 μL min^{-1}, which was roughly estimated using a Hagen–Poiseuille-based equation (note that the pressure drops calculated assuming laminar flow in the cylindrical configuration are in good agreement with the experimental measurements):

$$\Delta P = -128 \frac{\mu Q}{\pi d_{\mathrm{H}}^{4}} L \quad (1)$$

where ΔP is the pressure drop (Pa), L the channel length (m), μ the viscosity (Pa s), Q the volumetric flow rate (m^3 s^{-1}) and d_{H} the hydraulic diameter (m).

To guarantee mixing quality and fluid temperature, the microsystem has three different zones:[10] inlet/outlet zone, mixing zone and analysis zone (see Fig. 1).

The fluids enter at room temperature in the inlet/outlet zone and are later allowed to mix, while temperature increases from room temperature to the working temperature. Finally, the fluid mixture reaches the operating conditions before entering in the analysis zone, where it is characterized.

In order to study binary and ternary mixtures, the microsystem includes three inlets and two T-junction mixing points (see Fig. 2). The fluid inlets are kept with mitered 90° elbows with sharp bends in order to enhance fluid mixture by generating vortex at the corners. To study binary mixtures, one of the inlets is plugged. This approach allows validation of the experimental set-up for binary and ternary mixtures separately.

The microsystem was connected to the external set-up using a compression module described elsewhere.[10]

Experimental set-up

The general set-up is described in Fig. 2. Briefly, the flow rates are controlled by three high-pressure piston pumps (ISCO® 100DM), while a back pressure regulator (Equilibar® ULF) placed downstream is used to maintain a constant pressure in the microsystem. Finally, temperature is controlled within a ±0.1 K interval by a EuroTherm® 3200. The microdevice is heated with an electrical resistance of 200 W contacting its silicon backside to guarantee a constant sufficient heat transfer at temperatures above 380 K to compensate for

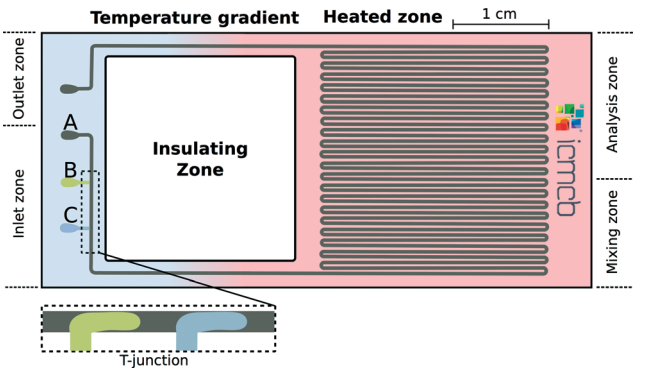

Fig. 1 Schematic of the microfluidic device with the three different zones. A, B and C inlets represent generic fluids.

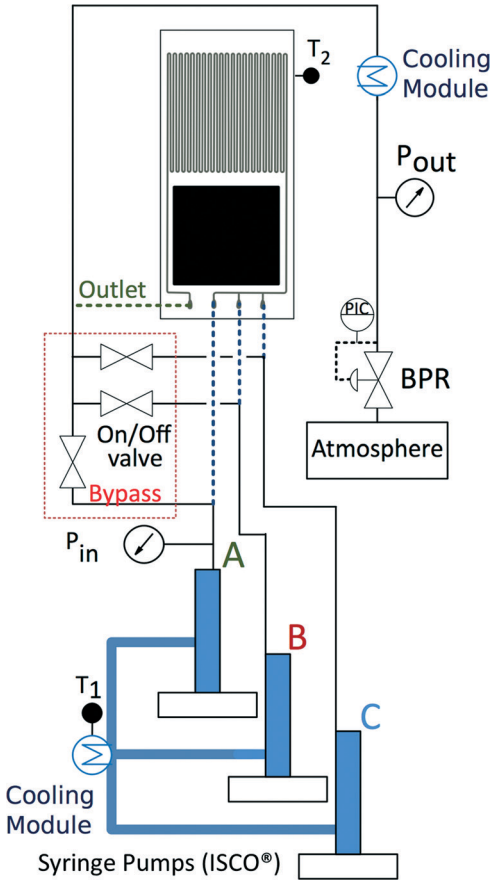

Fig. 2 Schematic diagram of a multiphasic microfluidic installation with a bypass line.

convective heat losses. To monitor the temperature within the full set-up, two K-type thermocouples are used to give the temperatures of (i) the fluids in the piston pumps thermostated with a recirculating cooling fluid, (T_1), and (ii) the working part of the microsystem (being put in direct contact with the backside of the microsystem), T_2. To monitor the pressure, two pressure transducers are placed upstream and downstream the microsystem. To guarantee the exact same measurement conditions, both pressure sensors were immersed in a constant temperature bath (50/50 wt% ethylene glycol/water) at 300 K. Analyses were conducted within a temperature range of 300 to 500 K and a pressure range of 60 to 150 bar.

A bypass line was also added to run the set-up in dynamic stop-flow mode (see details below).

To construct the thermodynamic diagrams, several movies were recorded with Phantom® Version 9.1 at different capturing velocities. For bubble formation and nucleation, movies were captured at 300 fps (1632 × 1200). For visualizing equilibrium evolutions, movies were captured between 4 and 40 fps (1632 × 1200). The high-speed camera is coupled with a Zeiss Axiovert 200 M inverted microscope equipped with a 5× objective.

3. Microfluidic strategy to build *P–T* phase diagrams

Principle: bubble and dew point detection

In order to construct a multicomponent *P–T* diagram, our approach is based on bubble and dew point on chip optical detection to access the phase envelope. Initially, a fluid mixture with a particular composition is introduced at equilibrium within the microsystem, displaying multiphasic liquid–vapor, *i.e.*, droplets/bubbles are formed inside the microchannel and can be easily observed (see Fig. 3-a-C*). Starting from these initial conditions, the temperature was subjected to variations under isobaric conditions to find the bubble and dew points. This means that the mixture turns to a fully miscible mixture (Fig. 3-a-A*) by crossing the phase envelope in the (P,T) projection of the phase diagram. This process can be viewed as the transition from the 2-phase to the 1-phase region. The bubble point (Fig. 3-a-B*) corresponds to a temperature value (at a given pressure) where the first bubble starts forming in the fluid medium. Similarly, the dew point (Fig. 3-a-D*) corresponds to the temperature (at a given pressure) where the last bubble disappears. After finding these points, the pressure was increased and the process was repeated. This loop method was carried out until the maxcondenbar (MCB) point is found, which is located at the maximum pressure of a *P–T* envelope (Fig. 3-b). After finding the MCB, the loop method was carried out until the maxcondentherm (MCT) is found, which is the maximum temperature of a *P–T* envelope (Fig. 3-b). Then, to determine the critical point, it is worth noting that the critical pressure (see Fig. 3-b, left) is located between the MCT and the MCB pressures ($P_{MCT} < P_c < P_{MCB}$).[20] By definition, the critical point is the junction between bubble and dew curves (see Fig. 3-b). This means that if $P < P_c$ there is a dew point and a bubble point; however, for $P > P_c$, we will have either two dew points (lower and upper) or two bubble points (lower and upper). The lower and upper bubble points and dew points are easy to spot in microfluidics, as exemplified in Fig. 4 (see also movies 1 to 4 in the ESI†).

Repeating the proposed method for various compositions and linking the critical points to one another allow determination of the mixture critical locus curve, as exemplified in Fig. 3-c for a binary CO_2–cyclohexane (CYC) mixture.

The microsystem can be operated in stop-flow (isochoric) or continuous flow mode. In isochoric systems, the pressure is directly controlled by temperature variations,[21] *e.g.* increasing temperature leads to increasing fluid pressure. These approaches could lack of flexibility when targeting the fast screening of phase behavior. On the contrary, continuous microflow mode allows for fast screening of the operating conditions (temperature, pressure, composition), but leads to poor precision over the system operating pressure due to the induced pressure drop inside the microchannels.

To overcome these limitations, our strategy is to operate the microsystem in a so-called dynamic stop-flow mode

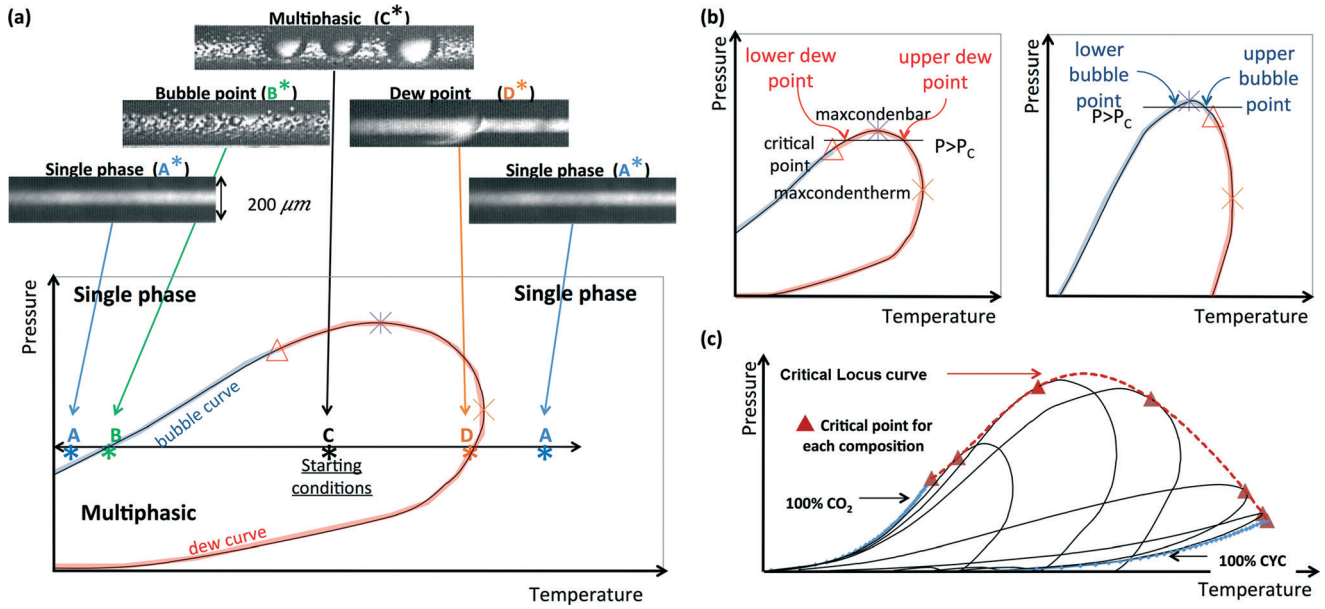

Fig. 3 (a) General loop method for building a *P–T* phase diagram through bubble and dew point detection and phase envelope construction. The bubble and dew points were determined by increasing or decreasing the temperature from the initial conditions to isobaric conditions. The images were captured at 4 fps for a mixture of CO_2 + CYC. (b) Scheme of the critical point based on whether it is located before or after the maxcondenbar (c) General description of a binary mixture critical locus (CO_2–CYC: type I-a mixture[24]).

(see the next section). In this regime, the fluid is completely stopped (no induced pressure drop), but is not confined to a specific volume, which means that *P–T* parameters can be changed independently. This ensures an improved precision over the operating conditions, making it ideal to do precise and fast phase behavior studies.

The dynamic stop-flow concept for fast screening

The dynamic stop-flow approach takes advantage of an open system – similar to the continuous flow regime – but the fluid is in a no-motion status. The concept developed behind this method is based on hydrodynamic resistance. Flowing through a small hydraulic diameter (d_H) tubing leads to higher hydrodynamic resistance than flowing through a tube with a larger hydraulic diameter (the fluidic resistance varies as d_H^4, see eqn (1)). Therefore, bypassing the microsystem with a large hydraulic diameter tubing (Fig. 5) forces the fluid to select the lower hydrodynamic resistance line.

Indeed, by considering the Hagen–Poiseuille equation (eqn (1)) for equal tubing lengths, we can express the flow rate ratio as the inverse of the fluidic resistance ratio and as the hydraulic diameter ratio raised to the power of 4 (eqn (2)):

$$\frac{Q_A}{Q_B} = \frac{R_{\mu system}}{R_{Bypass}} \approx \left(\frac{d_{H\,Bypass}}{d_{H\,\mu system}} \right)^4 \quad (2)$$

where Q_A and Q_B are the volumetric flow rates in each section (bypass and microsystem), respectively, R is the fluidic resistance and d_H is the hydraulic diameter.

Considering our set-up, the hydraulic diameters are 133 μm and 750 μm for the microsystem and the bypass, respectively. Thus, the flow rate ratio between the bypass and the microsystem line is ~10^3. In other words, at the T-junction, the fluid will always largely flow preferentially into the bypass line ($Q_A \gg Q_B$), thus flowing around the microsystem without disturbing the fluid mixture inside it.

In a typical experiment, pure fluids first mix in the desired proportions while flowing through the microsystem until the upstream pressure is stable (Q_{Total} = 50 μL min^{-1}, bypass valves are closed, meaning Q_A = 0 μL min^{-1}). This step lasts from 1 to 10 min depending on the overall compressibility of the considered fluid mixture. When the bypass valves are opened, the mixture inside the microsystem is kept in a quasi no-motion state (Q_A ~ 50 μL min^{-1}, Q_B ~ 0.05 μL min^{-1}). In order to prove the concept, a flow of CO_2 + CYC was introduced into the microsystem at a velocity of ~8×10^{-2} m s^{-1}. Then, the bypass valves were opened, which led to a small decrease of the upstream pressure sensor, since the pressure drop is smaller in the bypass line, and the fluid starts to be in a quasi no-motion state (ESI† movie 5).

To observe fluid flow inside the microchannel in continuous mode with some details, it is necessary to capture movies with a minimum of 300 fps (Fig. 6-a). On the contrary, in the case of quasi no-motion flow, 4 fps is enough and it is perfectly possible to visualize in detail the size of each bubble (Fig. 6-b).

Each isobaric set of experiments to cover the full range of temperatures typically takes less than 5 minutes (temperature variation is almost instantaneous). When temperature rises inside the system, the fluid will expand and the volume variation will be expelled by the system into the bypass line, avoiding pressure variations inside the microsystem. Changing the *P–T* conditions destabilizes the stationary regime of the system, inducing slight movements in the fluid

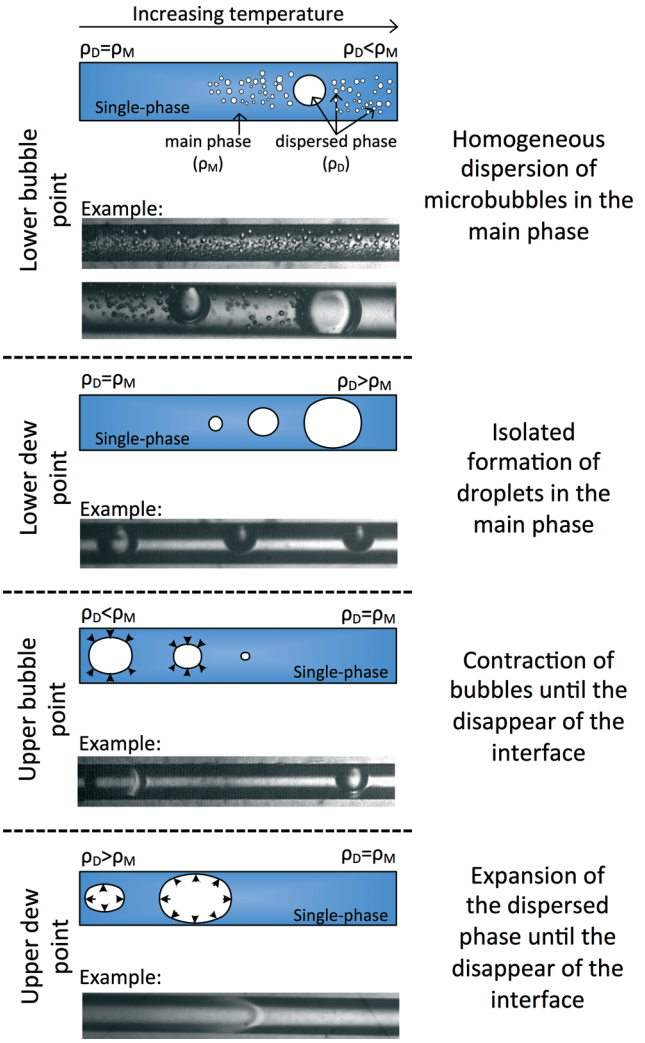

Fig. 4 Schematic of the point detection of the different behavior of the medium at $P > P_C$. The videos of each point can be found in the ESI.† The variable ρ represents the density of the fluid.

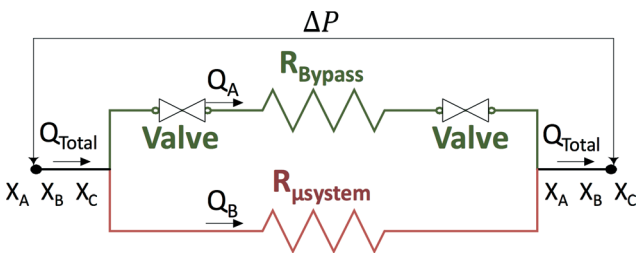

Fig. 5 System flow resistance circuit that one fluid undergoes in dynamic stop-flow mode.

until a new stationary regime is reached. Between stationary states, the bubbles' appearance, growth and disappearance can be easily investigated (Fig. 6 and ESI† movie 6).

In the transition between stationary states the bubbles/droplets increase or decrease in size, giving opportunity to extend the concept proposed in this paper to study *PVT* diagrams.

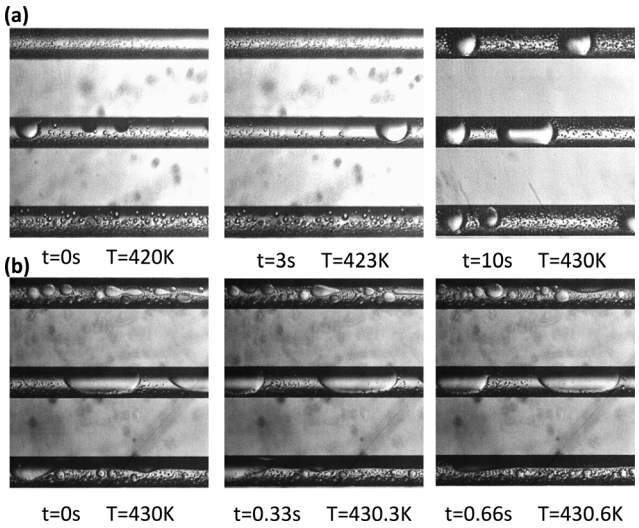

Fig. 6 Volume variation of the bubbles during a temperature increase. The bubbles are trapped into the microsystem, having a molar composition of 24% cyclohexane and 76% CO_2 at P = 138 bar. (a) Images captured at 300 fps using continuous flow mode and (b) images captured at 4 fps using dynamic stop-flow mode.

4. Results and discussion

Set-up reliability and *P–T* diagrams for binary CO_2–alkane mixtures

To check the reliability of our approach, two benchmark binary mixtures were considered: CO_2 + cyclohexane and CO_2 + pentane, for which literature data are available, allowing estimation of the set-up performance. Furthermore, the critical locus curve in mixtures of hydrocarbons and CO_2 is commonly of type II from the Scott and Van Konynenburg classification system.[22,23] In other words, these binary fluid mixtures only have a heterogeneous liquid–gas equilibrium and a liquid–gas critical locus curve between the critical points of each pure component. Note, however, that it is also possible to have a liquid–liquid heterogeneous equilibrium.[20]

To obtain a *P–T* phase envelope, the system was first placed under equilibrium conditions. Then, the procedure described previously was followed in order to determine the bubble and dew points. Fig. 7 presents *P–T* miscibility diagrams obtained for some selected CO_2 + pentane and CO_2 + cyclohexane compositions. The critical point for each composition can be found using the above-described procedure. The evolution of the critical pressure and temperature as a function of mixture composition was then determined based on the critical points obtained from the *P–T* diagrams; this curve was directly compared with literature and PREOS-calculated data (Fig. 8). Details about the PREOS calculations of critical points can be found in the ESI.†

Compared to the literature data, the obtained values have an average relative deviation of 2% and a maximum relative deviation of 4%. The main contribution to the deviation value is the composition variation at the system inlet, *i.e.*, small pump flow rate variations change the overall system

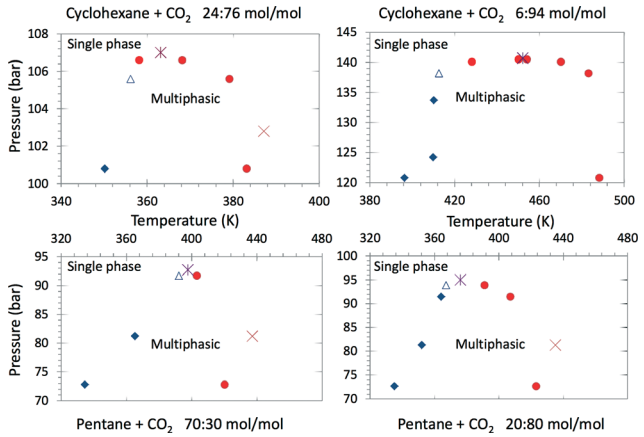

Fig. 7 *P–T* miscibility diagrams for binary CO_2 + cyclohexane and CO_2 + pentane mixtures obtained through the microfluidic approach. ◆ Bubble points; ● dew points; ✳ Maxcondenbar; × Maxcondentherm; △ Mixture critical points.

composition, making it possible to have slight deviations in the critical temperature and pressure. However, the excellent overall agreement of the results with the literature proves that our approach can be used to obtain critical data for binary mixtures.

From binary to ternary/quaternary diagrams

To verify that the concept can be used for more complex mixtures, a quaternary mixture, CO_2 + propylene + propane + H_2, was chosen as a model mixture. Such a system is representative of a hydrogenation reaction of propylene by hydrogen in CO_2 generating propane. The addition of hydrogen dramatically complicates the system, since this compressible fluid can interact with all three other species.

To simplify the system, we fixed the propylene/propane molar ratio to 93 : 7. We first determine the CO_2 + propylene + propane ternary critical locus curve to obtain a pre-validation step before investigating the quaternary system including hydrogen. The obtained experimental results were later compared with the numerical results obtained through the Peng–Robinson cubic equation of state (Fig. 9).

In the case of CO_2 + propylene + propane, the results are in excellent agreement with the calculated data, having an average relative deviation of 2% for critical temperature and pressure.

Note, however, that the calculated data strongly depend on the binary interaction parameter k_{ij}. In a ternary mixture, three k_{ij} have to be considered; therefore, inaccurate binary interaction parameters strongly influence the PREOS modeling results. The PREOS can give incoherent results when using k_{ij} that are not adapted to the working temperatures. Switching from PREOS to PPR78 can address this limitation by considering temperature-dependent k_{ij} obtained through a group contribution method, as previously reported.[27,28]

We later introduce H_2 into the mixture to investigate the quaternary phase diagram (CO_2 + propylene + propane + H_2). Using the same microfluidic approach, the *P–T* phase diagrams were plotted and the critical locus was determined as a function of the molar fraction of CO_2 (Fig. 10).

Given the complexity of such a mixture, modeling is not straightforward. However, our approach can be used to back calculate the various binary interaction parameters k_{ij} (required for the EOS calculations).

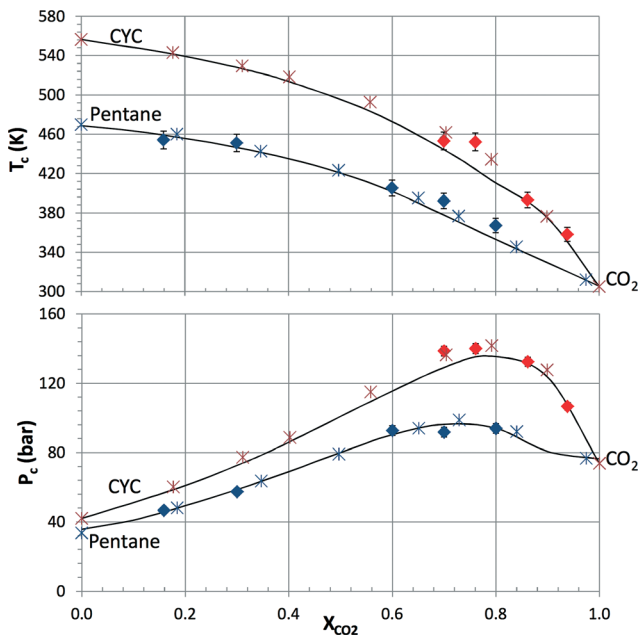

Fig. 8 Critical points for binary CO_2 + CYC and CO_2 + pentane mixtures. ♦ On-chip experimental results; ✳ literature data: CO_2 + CYC from Zhang *et al.* (2005);[24] CO_2 + pentane from Cheng *et al.* (1989);[25] and — PREOS results, using Heidemann *et al.* algorithm[26] (CYC + CO_2 k_{ij} = −0.05; pentane + CO_2 k_{ij} = 0.122).

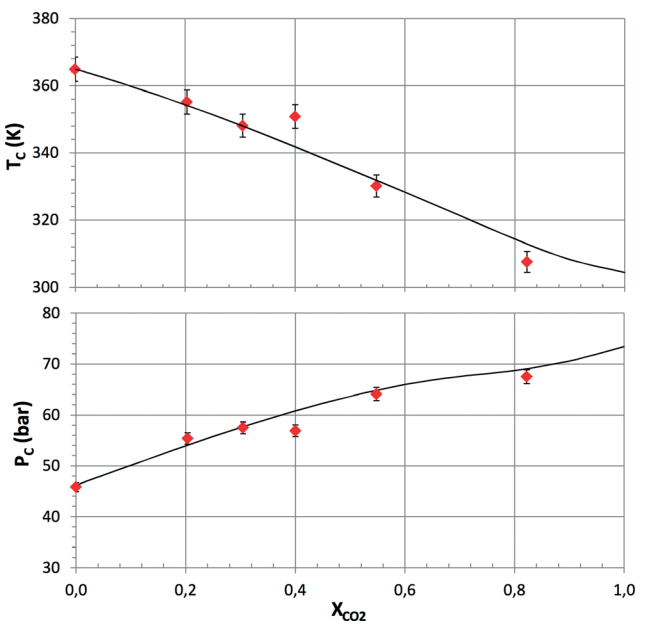

Fig. 9 Critical points for the ternary CO_2 + propylene + propane mixture (propylene/propane molar ratio fixed at 93 : 7). ◆ On-chip experimental results; — PREOS results for CO_2 + propylene + propane (CO_2 + propylene k_{ij} = 0.067; propylene + propane k_{ij} = 0.00830; propane + CO_2 k_{ij} = 0.1241).

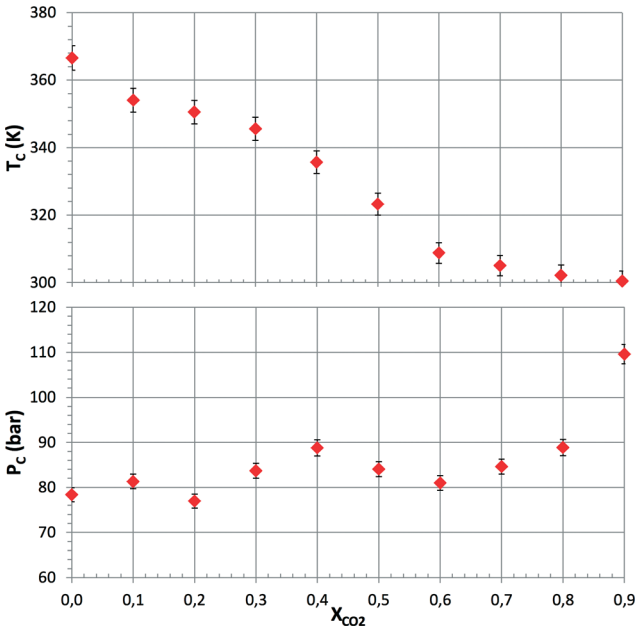

Fig. 10 Critical points for the quaternary CO_2 + propylene + propane + H_2 mixture with a constant 10% molar composition of hydrogen and constant propylene-to-propane molar ratio of 93 : 7. ♦ On-chip experimental results.

Conclusions

A microfluidic-based approach was presented to determine the *P–T* phase diagrams of multicomponent mixtures. This method couples an on-chip optical detection of both bubble and dew points with a so-called dynamic stop-flow mode for fast screening of the operating parameters (temperature, pressure, composition). This regime was created using a bypass line, making it possible to maintain a constant pressure inside the system while tuning the temperature.

We demonstrate that this strategy can provide accurate thermodynamic data for multicomponent mixtures, which were compared to PREOS-calculated and literature data. Additionally, this microfluidic approach can work very efficiently (typically 5 times faster than conventional HPOC methods), taking advantage of (i) the fast heat and mass transfer, (ii) the easy control of all the set-up operating parameters and (iii) the use of a dynamic stop-flow mode, which can provide all of the advantages of a quasi no-motion fluid in an open system. This ease of operation allows for accessing data that can later feed EOS modeling, in particular through the back calculation of binary interaction coefficients (k_{ij}). Although the presented method was only used to investigate *P–T* diagrams, it is also possible to envision building *PVT* diagrams, taking into account the void fraction, as previously reported.[14]

Acknowledgements

The authors would like to thank the IFPEN, the ANR (through the SEED "CGSμLab" project and the international "Sustainable Manufacturing" project), the CNES and the Région Aquitaine for financial support.

Notes and references

1 B. Kerler and A. Martin, *Catal. Today*, 2000, **61**, 9–17.
2 F. Meyer, M. Stamenic, I. Zizovic and R. Eggers, *J. Supercrit. Fluids*, 2012, **72**, 140–149.
3 A. Fourcault, B. García-Jarana, J. Sánchez-Oneto, F. Marias and J. R. Portela, *Chem. Eng. J.*, 2009, **152**, 227–233.
4 N. Liu, C. Aymonier, C. Lecoutre, Y. Garrabos and S. Marre, *Chem. Phys. Lett.*, 2012, **551**, 139–143.
5 P. Carlès, *J. Supercrit. Fluids*, 2010, **53**, 2–11.
6 S.-X. Hou, G. C. Maitland and J. P. M. Trusler, *J. Supercrit. Fluids*, 2013, **73**, 87–96.
7 J. Ke, B. Han and M. George, *J. Am. Chem. Soc.*, 2001, **123**, 3661–3670.
8 B. A. Stradi, M. A. Stadtherr and J. F. Brennecke, *J. Supercrit. Fluids*, 2001, **20**, 1–13.
9 N. Juntarachat, P. D. Beltran Moreno, S. Bello, R. Privat and J.-N. Jaubert, *J. Supercrit. Fluids*, 2012, **68**, 25–30.
10 S. Marre, A. Adamo, S. Basak, C. Aymonier and K. F. Jensen, *Ind. Eng. Chem. Res.*, 2010, **49**, 11310–11320.
11 S. Marre, Y. Roig and C. Aymonier, *J. Supercrit. Fluids*, 2012, **66**, 251–264.
12 R. Guillaument, A. Erriguible, C. Aymonier, S. Marre and P. Subra-Paternault, *J. Supercrit. Fluids*, 2013, **81**, 15–22.
13 K. W. Oh, K. Lee, B. Ahn and E. P. Furlani, *Lab Chip*, 2012, **12**, 515–545.
14 F. Mostowfi, S. Molla and P. Tabeling, *Lab Chip*, 2012, **12**, 4381–4387.
15 A. Urakawa, F. Trachsel, P. R. von Rohr and A. Baiker, *Analyst*, 2008, **133**, 1352–1354.
16 T. Gervais, J. El-Ali, A. Günther and K. F. Jensen, *Lab Chip*, 2006, **6**, 500–507.
17 K. Shinohara, Y. Sugii, A. Aota, A. Hibara, M. Tokeshi, T. Kitamori and K. Okamoto, *Meas. Sci. Technol.*, 2004, **15**, 1965–1970.
18 T. Gervais and K. F. Jensen, *Chem. Eng. Sci.*, 2006, **61**, 1102–1121.
19 R. Fisher, M. K. Shah, D. Eskin, K. Schmidt, A. Singh, S. Molla and F. Mostowfi, *Lab Chip*, 2013, **13**, 2623–2633.
20 R. Privat and J.-N. Jaubert, *Chem. Eng. Res. Des.*, 2013, **91**, 1807–1839.
21 X. Wang, I.-M. Chou, W. Hu, R. C. Burruss, Q. Sun and Y. Song, *Geochim. Cosmochim. Acta*, 2011, **75**, 4080–4093.
22 S. Vitu, R. Privat, J.-N. Jaubert and F. Mutelet, *J. Supercrit. Fluids*, 2008, **45**, 1–26.
23 P. H. Van Konynenburg and R. L. Scott, *Philos. Trans. R. Soc., A*, 1980, **298**, 495–540.
24 R. Zhang, Z. Qin, G. Wang and M. Dong, *J. Chem. Eng. Data*, 2005, **50**, 1414–1418.
25 H. Cheng, M. E. P. de Fernandez, J. A. Zollweg and W. B. Streett, *J. Chem. Eng. Data*, 1989, 319–323.
26 R. Heidemann and A. Khalil, *AIChE J.*, 1980, **26**, 769.
27 J.-W. Qian, J.-N. Jaubert and R. Privat, *Fluid Phase Equilib.*, 2013, **354**, 212–235.
28 J.-W. Qian, J.-N. Jaubert and R. Privat, *J. Supercrit. Fluids*, 2013, **75**, 58–71.